Tumor cell-driven extracellular matrix remodeling enables haptotaxis during metastatic progression

Tumor cell-driven extracellular matrix remodeling drives haptotaxis during metastatic progression

Madeleine J. Oudin[1], Oliver Jonas[1], Tatsiana Kosciuk[1], Liliane C. Broye[1], Bruna C. Guido[1], Jeff Wyckoff[1], Daisy Riquelme[1], John M. Lamar[1], Sreeja B. Asokan[3], Charlie Whittaker[1], Duanduan Ma[1], Robert Langer[1], Michael J. Cima[1], Kari B. Wisinski[7], Richard O. Hynes[1,5,6], Douglas A. Lauffenburger[1,2], Patricia J. Keely[4], James E. Bear[3,6], Frank B. Gertler*[1,5]

[1] David H. Koch Institute for Integrative Cancer Research, MIT, Cambridge, MA, USA
[2] Department of Biological Engineering, MIT, Cambridge, MA, USA
[3] Lineberger Comprehensive Cancer Center, UNC Chapel Hill, Chapel Hill, NC, USA
[4] Department of Cell and Regenerative Biology, University of Wisconsin Madison, Madison, WI, USA
[5] Department of Biology, MIT, Cambridge, MA, USA
[6] Howard Hughes Medical Institute
[7] Department of Medicine, University of Wisconsin Carbone Cancer Center, Madison, WI, USA

Running Title: Haptotaxis and metastasis

Keywords: breast cancer, cell adhesion and extracellular matrix, cell motility and migration, imaging of tumor progression and metastasis, metastasis/metastasis genes/metastasis models, tumor markers and detection of metastasis, haptotaxis, Mena, Ena/VASP

Abbreviations list:

CI confidence interval, ECM extracellular matrix, EGF epidermal growth factor, GFP green fluorescent protein, FAK focal adhesion kinase, FX focal complexes, FMI forward migration index, FN fibronectin, IP immunoprecipitation, HR hazard ratio, LN laminin, MMP matrix metalloproteinase, RTK receptor tyrosine kinase, SHG second harmonic generation, TCGA The Cancer Genome Atlas, TMA tissue microarray, VN vitronectin.

Financial support:

This work was supported by a DoD Breast Cancer Research Program post-doctoral fellowship to W81XWH-12-1-0031 to MJO, funds from the Ludwig Center at MIT to FBG and ROH, NIH grant U54-CA112967 to FBG, ROH and DAL, HHMI funding to ROH, NIH grants R01 CA142833, R01 CA114462 and U01 CA143069 to PJK, a Science without borders/CNPq fellowship to BCG, the Koch Institute Frontier Award from the Kathy and Kurt Marble Research Fund to FBG, MJC and RL, funds from the Prostate Cancer Foundation to OJ and RL and the Koch Institute NCI core grant P30-CA14051.

*Corresponding author:

Frank B. Gertler

Koch Institute for Integrative Cancer Research

MIT 76-361a

77 Massachusetts Ave

Cambridge, MA 02139

617-253-5511

fgertler@mit.edu

Conflict of interest: FBG is on the advisory board for MetaStat. MetaStat did not provide any direct funding for this work.

Abstract

Fibronectin (FN) is a major component of the tumor microenvironment, but its role in promoting metastasis is incompletely understood. Here we show that FN gradients elicit directional movement of breast cancer cells, *in vitro* and *in vivo*. Haptotaxis on FN gradients requires direct interaction between α5β1 integrin and Mena, an actin regulator, and involves increases in focal complex signaling and tumor-cell-mediated extracellular matrix (ECM) remodeling. Compared to Mena, higher levels of the pro-metastatic Mena^{INV} isoform associate with α5, which enables 3D haptotaxis of tumor cells towards the high FN concentrations typically present in perivascular space and in the periphery of breast tumor tissue. Mena^{INV} and FN levels were correlated in two breast cancer cohorts, and high levels of Mena^{INV} were significantly associated with increased tumor recurrence as well as decreased patient survival. Our results identify a novel tumor-cell-intrinsic mechanism that promotes metastasis through ECM remodeling and ECM guided directional migration.

Statement of significance

Here, we provide new insight into how tumor cell: ECM interactions generate signals and structures that promote directed tumor cell migration, a critical component of metastasis. Our results identify a tumor-cell-intrinsic mechanism driven by the actin regulatory protein Mena, that promotes ECM remodeling and haptotaxis along FN gradients.

Introduction

The tissue microenvironment is composed of stromal cells and extracellular matrix (ECM) and is known to contribute to tumor progression(1). This compartment is rich in substrate-bound and soluble cues, and provides both the structure and signals that promote tumor cell proliferation, survival and invasion(2). The most abundant ECM proteins in mouse metastatic breast tumors are fibronectin (FN) and collagens(3). In breast cancer patients, collagen organization has high prognostic value(4,5) and increased FN correlates with disease progression and mortality(6,7). The context and mechanisms by which tumor cells sense and respond to changes in ECM abundance and architecture during invasion and metastasis, however, remain poorly understood.

Cancer cells can respond to a variety of cues in order to locally invade and metastasize. Growth factor-mediated chemotaxis is known to be important for local invasion and metastasis(8). Far less is known about haptotaxis, a process in which cell migration is guided by gradients of surface-bound molecules such as ECM. This is particularly relevant to cancer, where the amount of FN within tumors can vary greatly, with high concentrations of FN typically found near blood vessels, tumor periphery and in metastatic sites(9,10). While FN can activate intracellular signaling pathways via integrins(11), the predominant class of surface adhesion receptors, cells can also remodel the ECM, for example, by driving integrin-mediated assembly of soluble FN into fibrils(12). FN is also known to play an important role in collagen fibrillogenesis(13). Bi-directional communication between cells and ECM cues regulates cell behavior as well as the composition and structure of the surrounding ECM.

Mena, a member of the Ena/VASP family of actin filament elongation factors, is upregulated in various cancers and undergoes alternative splicing during breast cancer progression(14). Mena binds to the C-terminal end of the cytoplasmic tail of the integrin

α5 via an LERER repeat domain absent from other Ena/VASP proteins(15). In fibroblasts, Mena regulates both outside-in and inside-out signaling at focal complexes via its interaction with α5 (15). Mena^{INV}, an alternatively spliced isoform containing a 19-amino acid inclusion (encoded by the "INV" exon), is expressed in aggressive tumor cell subpopulations(16). Mena^{INV} expression promotes metastasis by increasing sensitivity to EGF(17) and the efficiency of matrix degradation, invasion and intravasation (18). Together, these findings led us to hypothesize that the ECM may also play an important role in Mena/Mena^{INV}-driven metastasis. Using pre-clinical models and analysis of patient samples, we describe a previously unappreciated mechanism of metastasis, where upregulation of Mena and its invasive isoform endows tumor cells with the ability to migrate up FN gradients and fashion their own pathway towards the bloodstream.

Results

Mena drives haptotaxis of tumor cells on FN gradients via its interactions with α5β1 and F-actin

Based on the recent finding that Mena interacts with the cytoplasmic tail of one of the main FN receptors α5, we hypothesized that Mena may be involved in directional migration responses to gradients of FN. Using a recently developed microfluidic device, we studied cells migrating on FN gradients by time-lapse imaging, and quantified their forward migration index (FMI) to assess haptotaxis (Fig1A) (19,20). First, MV^{D7} fibroblasts, which lack all three Ena/VASP proteins (Mena, VASP and EVL(21)) migrated actively in the device, however, they failed to haptotax on the FN gradient. Interestingly, Mena-, but not VASP-, EVL- expressing MV^{D7} cells exhibited a robust haptotactic response and migrated up the FN gradient (Fig1B), even though expression of each of the three Ena/VASP proteins had previously reported, similar effects on cell speed (21) (FigS1A).

We next examined Mena-dependent effects on haptotaxis of breast cancer cells. In serum-free conditions, MDAMB231 cells become enriched on the FN coated undersides of porous filters in transwell assays(22), however, we found that this cell type failed to exhibit directional movement on FN gradients (Fig1C). MDAMB231 cell lines stably expressing GFP-tagged Mena or control-GFP construct at levels similar to those seen in invading cells *in vivo* were generated (referred to as 231-Control or Mena) (23)(FigS1B,C). Ectopic expression of Mena enabled significant haptotactic responses on 2D gradients of FN, but not of on 2D laminin (LN) or vitronectin (VN) gradients (Fig1C), without affecting cell speed (FigS1D). Varying the concentration of either VN or LN affected the speed of MDAMB231 and 231-Mena cells, but failed to elicit significant haptotactic responses at any concentration tested (FigS1D-G).

In 3D collagen gels with FN gradients, Mena expression also induced a strong haptotactic response (Fig1D), independently of velocity (FigS1E). While the exact concentration of FN in tumors is unknown, FN is expressed by tumor and stromal cells, and accumulates in the perivascular area via leakage from the bloodstream, where FN levels as high as 400μg/ml have been observed(24). Due to the heterogeneous levels of FN found in tumors, we studied haptotaxis 3D collagen gels in response to gradients generated from different source concentrations of FN. In high levels of FN (up to 500μg/ml), 231-GFP and 231-Mena cells were unable to migrate up the FN gradient and instead migrated away from the FN source, indicating that the pro-haptotactic effect of Mena on FN gradients is concentration-dependent.

The role of integrins in FN haptotaxis, in particular the two major FN-binding integrins, α5β1 and αvβ3 integrins, remains poorly understood. Inhibition of α5β1 by the function blocking antibody P1D6, but not of αvβ3 by Cilengitide (25), blocked haptotaxis of 231-Mena cells (FMI values decreased by over 90%; Fig1E), indicating that Mena-driven FN haptotaxis requires α5β1 signaling specifically. We tested whether Mena's ability to bind α5 via its LERER domain was required for Mena to support haptotaxis (Fig1F). MDAMB231 cell lines stably expressing GFP-tagged Mena in which the LERER domain was deleted to abrogate the interaction between Mena and α5 (231-MenaΔLERER)(15) showed no apparent defects in protein localization (as judged by the GFP-tag), cell morphology, cell area or proliferation on plastic at steady state (FigS1B,C,F,G). 231-MenaΔLERER cells failed to haptotax in 3D to FN (FMIs reduced by over 90%; Fig1G), however, their migration velocity was similar to cells expressing intact Mena (Fig1H). Similar results were obtained in MV^{D7} fibroblasts on a 2D FN gradient (FigS1H,I). Previously, we found that, while the LERER domain was required for fibroblast spreading on FN, the F-actin binding site in Mena was

dispensable(15)(Fig1F). Therefore, we investigated the role of the F-actin binding (FAB) site of Mena in FN-driven haptotaxis. 231-MenaΔFAB cells failed to haptotax in a FN gradient in a 3D collagen gel (Fig1G), while also displaying slight reductions in cell velocity (Fig1H). Overall, these data demonstrate that sensing changes in FN concentrations depends on α5β1 function, as well as the ability of Mena to bind α5 and to F-actin.

Mena^{INV} drives haptotaxis in high FN concentrations *in vitro* and *in vivo*

We next investigated the role of the Mena^{INV} isoform in driving haptotaxis. Cultured cells show little to no detectable Mena^{INV} compared to spontaneous or xenograft mammary tumors(26). MDAMB231 and SUM159 cell lines stably expressing GFP-tagged Mena^{INV} or Mena^{INV}ΔLERER constructs at levels similar to those generated for Mena (referred to as 231- or 159-Mena^{INV} or Mena^{INV}ΔLERER) were made (FigS1B,C). Surprisingly, unlike Mena, Mena^{INV} enabled tumor cell haptotaxis through gradients of high FN concentrations, even up to 500 μg/ml (Fig2A), effects that were independent of velocity (FigS2A,B). In contrast, varied concentration gradients of either VN or LN failed to elicit significant haptotactic responses by 231-Mena^{INV} cells, suggesting this response was specific to FN (FigS2D,E). Inhibition of α5β1, but not of αvβ3 blocked haptotaxis of 231-Mena^{INV} cells (Fig2B,S2C). Mena^{INV} also binds the cytoplasmic tail of α5 directly via its LERER domain; we found that 231-Mena^{INV}ΔLERER and 231-Mena^{INV}ΔFAB cells also failed to haptotax in 3D to FN (Fig2B). These findings were confirmed in 2D and 3D collagen gels using SUM-159 cells expressing the different GFP-tagged Mena isoforms (FigS2F-I). Overall, these data suggest that expression of Mena^{INV} enables cells to haptotax at higher FN concentrations than Mena.

While upregulation of FN in aggressive tumors is thought to promote invasion and metastasis, whether FN gradients play a role in guiding tumor cell migration *in vivo* has not been established. Xenograft tumors were generated in in the mammary fat pad of immunocompromised mice using MDAMB231 and SUM159 cells. We assayed the ability of cells from the primary tumor to invade actively into microneedles loaded with collagen and increasing concentrations of FN(27). 231-Control tumor cells were not attracted to FN *in vivo* (Fig2C), while 231-Mena tumor cells exhibited a biphasic response with robust invasion by 231-Mena cells at intermediate FN concentrations, but little to no invasion into needles with either low or high FN concentrations (Fig2C). Interestingly, 231-Mena^{INV} cells were still attracted into the needles containing the high concentrations of FN (Fig2C). While Mena can promote invasion *in vivo* in response to intermediate FN gradients, Mena^{INV} allows tumor cells to migrate through substantially higher (2-fold greater) FN concentrations.

To visualize FN-driven haptotactic responses inside tumors, we used a microscale implantable device that allows for *in vivo* release of molecules in gradients(28). Devices filled with Rhodamine-labeled FN were implanted near the edges of MDAMB231 or SUM159 orthotopic tumors to generate high concentration FN gradients (Fig2D). Using intravital imaging, cell motility and FMIs were quantified in response to gradients of FN or to fluorescently labeled dextran similar of size to FN as a control (FigS2J). Expression of Mena^{INV}, but not Mena, in human MDAMB231 and SUM159 cells significantly increased the number of cells moving in the xenograft tumors an effect dependent on the interaction with α5β1 (FigS2L,M). In tumors implanted with FN-loaded devices, 231-Mena^{INV}, but not 231-Control or 231-Mena cells moved towards the FN gradient (Fig2E, representative images with cell tracks FigS2K and supplementary videos 1&2). In contrast, 231-MenaΔLERER and Mena^{INV}ΔLERER cells

did not. Similarly, cells in 159-Mena^{INV} tumors migrated towards the FN, an effect that was absent in 159-Control or 159-Mena^{INV}ΔLERER tumor cells (Fig2F). Altogether, using the needle collection assay and intravital imaging, we show for the first time that haptotaxis towards FN occurring *in vivo* is driven by Mena^{INV} and its interaction with α5.

Mena isoform expression correlates with FN and integrin α5 expression levels as well as outcome in human breast cancer patients

Previous work demonstrated that forced expression of Mena^{INV} drives metastasis in xenograft tumor models(17) and that Mena^{INV} mRNA levels, as detected by qPCR are relatively higher in cells that intravasate efficiently and in patients with high numbers of TMEM (a structure containing a tumor cell, macrophage and endothelial cell associated with the likelihood of metastasis in ER^{+}/Her2^{-} breast cancer patients) (29). However, the relationship between Mena^{INV} mRNA or protein levels and patient outcome in human breast cancer patients has not been investigated. First, we analyzed the 1060 breast cancer patients in the TCGA cohort with RNAseq and clinical data available (30). Since the INV exon was not annotated when the RNAseq data were first analyzed, we accessed the raw sequence data and mapped reads in each sample to all Mena exons. Separating patients into quartiles according to Mena expression failed to reveal any significant correlations between Mena levels (judged by levels of constitutively-included exons) and overall survival in the entire TCGA breast cancer cohort (Fig S3A) or in the subset of patients with >10yr follow-up (Fig 3A). However, patients with high levels (top 1/4) of Mena^{INV} mRNA (as assessed by the abundance of INV exon sequence reads) exhibited significantly reduced survival compared to patients in each of the three lower quartiles of Mena^{INV} expression (Figs 3B, S3B). Similar results were found in the node-negative patient subgroup (FigS3E). Furthermore, both Cox and logistic regression

demonstrated that Mena^{INV} was a substantially stronger predictor of poor outcome in patients with 10-year follow up than Mena alone (Figs 3C,D, S3C,D); models combining Mena^{INV} and Mena expression levels failed to increase the predictive power beyond that of Mena^{INV}. We next studied how Mena^{INV} levels correlated with FN and α5 expression in this dataset. Overall Mena and Mena^{INV} expression were both significantly correlated with FN, and to a lesser degree α5 (FigS3F). In particular, in patients with >10yr follow-up, we observed a highly significant correlation between Mena, Mena^{INV} and FN or α5 in patients that succumbed to their disease, that was absent in surviving patients (FigS3G,H).

Using a newly developed antibody specific for Mena^{INV}(26), we then investigated the relationship between endogenous Mena^{INV}, α5 and FN protein using immunostaining in the MMTV-PyMT spontaneous mouse model of breast cancer(31) and in a previously characterized tissue microarray (TMA) of 300 patients(32). Both Mena and Mena^{INV} are expressed in PyMT tumors (Fig3E) and can be detected in cells that also express α5β1 (Fig3F). Mena^{INV} expression and distribution significantly correlated with that of FN in this model (Fig3G,H). We also found a significant correlation between FN and Mena^{INV} levels in the TMA (Fig3I,J). Similarly, in patients represented by the TMA, higher Mena^{INV} levels were significantly correlated with poor outcome (FigS3I). In addition, patients with recurrent disease, either local or at a distant site, had significantly higher levels of Mena^{INV} (Fig3K). Logistic regression analysis indicated that Mena^{INV} expression Mena^{INV} was a significant predictor of recurrence (Coefficient of 0.377, $p = 0.0186$). An average 4.6-fold increase in Mena^{INV} expression correlated with a 2-fold increase in the number of patients with recurrence (FigS3J,K). Further increases in Mena^{INV} expression did not correlate with further increases in recurrence, suggesting that even small increases in Mena^{INV} protein expression can affect recurrence. While mRNA levels of either Mena^{INV}

or FN alone did not correlate with time to disease recurrence, patients with high levels of *both* Mena^{INV} and FN showed a statistically significant decrease in time to recurrence (Fig3L). Together, these data provide the first evidence that Mena^{INV} RNA and protein levels correlate with tumor recurrence and survival and support a link between endogenous Mena^{INV}, α5 and FN expression in breast cancer patients.

To evaluate the role of Mena/Mena^{INV}-driven haptotaxis in metastasis, we quantified the number of spontaneous metastases in the lungs of mice with MDAMB231 and SUM159 xenografts. Mice were sacrificed when primary tumor size reached 1cm in diameter. Interestingly, the initial growth rate of 231- and 159-Mena^{INV}ΔLERER tumors was slower than that of tumors generated from the other cell lines (FigS4A,B). While there were only minor changes in proliferation levels as detected using the marker Ki67, 231-Mena^{INV}ΔLERER tumors had a 6-fold increase in levels of the apoptotic marker cleaved caspase-3 (FigS4D,E). This delay in tumor growth and increase in cell death could be rescued by co-injecting 231-Mena^{INV}ΔLERER cells with wild-type MDAMB231 cells expressing mCherry or by letting them grow for 12 weeks instead of 8 to reach 1cm in diameter (FigS4D,E). Expression of Mena^{INV} significantly increased the metastatic index in the lungs 5-fold in both human cell lines at 8 weeks, compared to control 231s (Fig3M-O). Deletion of the LERER region in both Mena and Mena^{INV} significantly decreased the lung metastatic index (Fig3N,O). Similar results were found in the poorly metastatic SUM159 cell line (Fig S4E). Similarly, depletion of all Mena isoforms in MDAMB231 cells using shRNA also delayed tumor growth, as well as decreasing tumor cell motility and metastasis (FigS4G-M). These data support a model whereby Mena/Mena^{INV}-driven α5-dependent haptotaxis plays a key role in promoting tumor metastasis.

Haptotaxis on FN gradients is dependent on signaling at focal complexes (FXs)

We next investigated the mechanism by which Mena isoforms drive haptotaxis at low and high FN concentrations. One way FN can support cell migration is by activating integrin-mediated intracellular signaling pathways at FXs that promote cell motility(11). When plated on 2D collagen and FN, both 231-Mena and 231-Mena^{INV} cells showed increases in cell area and in the number of α5-positive adhesions relative to control cells, or to cells plated on collagen only, an effect dependent on α5 activity as well as the α5-binding LERER domain (Fig4A-E). While 231-Mena^{INV} cells showed a 30% increase in both total and surface levels of α5, the steady state levels of αv, β1 and other integrins examined were unchanged (FigS5A-G). Furthermore, plating cells on FN also increased the levels of α5 within Mena-positive adhesions (indicated by the GFP tag), with 231-Mena^{INV} cells showing increased α5 levels relative 231-Mena cells (Fig4B,F). The FN-driven recruitment of α5 to Mena-positive adhesions was dependent on α5 activity as well as the LERER domain for both isoforms (Fig4F,G). 231-Mena^{INV}ΔLERER cells also had reduced number of Mena-positive adhesions (FigS5I).

Phosphorylation of several proteins at focal adhesions downstream of integrin activation, particularly focal adhesion kinase (FAK), is important for motility and tumorigenesis (11,33). Pharmacological inhibition of FAK inhibited Mena and Mena^{INV}-driven haptotaxis on low FN gradients (Fig4H). Immunofluorescence of haptotaxing cells revealed that both 231-Mena and Mena^{INV} cells show increased number of pFAK397-positive adhesions (Fig4I,J). In 231-Mena^{INV}ΔLERER or 231-Mena^{INV}ΔFAB cells, the number of pFAK397-positive adhesions in the cells was significantly lower than in 231-Mena^{INV} cells (Fig4K). When cells were plated on high FN gradients, only 231-Mena^{INV} cells haptotaxed (Fig S5J) and accordingly, these cells had a significant increase in the number of pFAK397-positive adhesions relative to 231-Mena or control cells (Fig4L).

These data suggest that outside-in activation of integrins and Mena-dependent FX signaling by FN is important for haptotaxis of tumor cells.

The differences between focal complex composition, signaling and haptotaxis arising from expression of Mena^{INV} vs. Mena prompted us to ask whether we could detect any relevant biochemical differences between the isoforms. Previously we demonstrated that Mena could be detected in complex with α5 by co-immunoprecipitiation (IP)(15). We performed α5 IPs to compare the amounts of Mena and Mena^{INV} in complex with α5, and reproducibly detected an average 2.2 fold greater level of Mena^{INV} compared to Mena by western blot of anti-α5 IPs (Fig4M,N). Thus inclusion of INV in Mena leads to significantly increased association with α5β1.

Mena^{INV}-driven ECM remodeling is required for 3D haptotaxis

FN could also support haptotaxis through its role in providing structural support for cells, particularly in 3D and in the presence of collagen. FN fibrillogenesis exposes cryptic binding sites in FN normally hidden in the globular form(12) and fibrillar FN can bind collagen and regulate its deposition and organization(13). 231-Mena and Mena^{INV} cells had increased number of protrusions in low FN gradients, while in high FN gradients, only 231-Mena^{INV} cells showed this phenotype (Fig S6A). Similarly, 231-Mena^{INV} cells were more elongated than Mena or Control cells in the presence of a FN gradient *in vivo*, an effect dependent on the interaction with α5 (FigS6B,C). We also found that 231-Mena^{INV} exhibited increased accumulation (20%) of FN (Fig5A,B) and collagen (Fig5A,C) at both low and high FN concentrations after 24 hrs, while neither 231-Mena nor 231-Control cells exhibited any significant accumulation of the two ECM proteins. FN-triggered outside-in signaling was insufficient to support Mena^{INV}-dependent haptotaxis in 3D gels, as 231-Mena^{INV} cells failed to haptotax on a gradient of FN7-11, a

fragment of FN that activates signaling via RGD-binding integrins, but cannot form fibrils (12) (Fig5D). Inhibition of fibrillogenesis by addition of a 70kD FN fragment that contains the cryptic FN- and collagen binding sites in FN (34) blocked Mena^{INV}-driven 3D haptotaxis (Fig5E). Therefore, the formation of FN fibrils is important for FN to evoke directional motility of tumor cells in 3D. Addition of the 70kD FN fragment to spreading 231-Mena^{INV} cells decreased the number of α5-positive adhesions as well as α5 recruitment to Mena^{INV}-positive adhesions (FigS6D-G), suggesting that fibrillar FN may enhance assembly of α5β1-containing adhesions.

In 231-Mena^{INV} cells, inhibition of α5β1 decreased accumulation of both FN and collagen, while inhibition of αvβ3 had little or no effect. 231- Mena^{INV}ΔLERER and 231-Mena^{INV}ΔFAB cells had decreased FN and collagen (Fig5F,G) accumulation around the cells. Inhibition of protease activity with the broad-spectrum matrix metalloproteinase (MMP) inhibitor BB94 had no effect on ECM reorganization, but inhibition of acto-myosin contractility by the ROCK inhibitor Y-27632 did decrease collagen and FN accumulation around the cells (FigS6H,I). These results indicate that Mena^{INV}-driven α5-dependent FN and collagen accumulation by the tumor cells themselves is important for haptotaxis.

Mena^{INV} expression drives collagen reorganization in tumors

Given the role of Mena^{INV} in driving ECM reorganization *in vitro*, the importance of FN for collagen fibrillogenesis(13), and recent published work showing that collagen organization can correlate with disease outcome(5), we next examined whether the changes in ECM accumulation observed short-term *in vitro* translated into significant changes in the structure and abundance of collagen *in vivo*. Using Second Harmonic Generation (SHG), we examined the structure and abundance of collagen in multiple tumors to investigate whether Mena and Mena^{INV} were associated with changes in

collagen abundance and organization *in vivo.* We examined the thickness of the collagen capsule surrounding the tumors. Intravital imaging of tumors revealed that deletion of the LERER in both 231-Mena and Mena^{INV} tumors lead to significantly thicker, collagen capsules (FigS6J). Similarly, knockdown of Mena in 231 cells also led to an increase in collagen thickness (FigS6K). Histological analysis of tumor sections showed that tumors in MMTV-PyMT mice null for Mena, known to have significantly lower levels of metastasis(35), showed significantly increased collagen levels, compared to wild-type mice (Fig6A,B). Endogenous Mena^{INV} levels in wild-type PyMT tumors were correlated with lower levels of collagen (Fig6C,D). In patients with high Mena^{INV} expression, there was significantly lower collagen signal than in patients with low Mena^{INV} expression (Fig6E,F). Together, these data suggest that highly invasive tumors arising from, or correlating with Mena^{INV} expression were associated with thinner collagen capsules, while the poorly metastatic tumors arising from Mena deficient cells were associated with thicker collagen capsules.

While the amount of collagen deposition surrounding tumor an important factor in local invasion, changes in collagen shape and orientation have also been linked with invasiveness. A lower density of collagen organized into straight fibers oriented perpendicularly to the edge of the tumor has been associated with poor outcome in a breast cancer cohort (5). Representative images of the collagen at the edge of the MDAMB231 and SUM159 xenograft tumors show 231-Control and 231-Mena tumors had dense, curly collagen fibers, organized in all directions relative to the tumor edge (Fig6G,H, FigS6L). However, 231-Mena^{INV} tumors displayed a significantly increased frequency of fibers orientated perpendicular to the tumor edge (Fig6G,H). 231-MenaΔLERER and 231-Mena^{INV}ΔLERER tumors had collagen fibers parallel to the tumor edge (FigS6L,M). Indeed, these tumors contained abundant collagen fibers with

very small angles relative to the tumor edge. Both phenotypes were also observed in tumors generated with SUM159 cells (Fig6G, S6N,O). Together, these results indicate that the initial Mena^{INV}-dependent changes in ECM accumulation observed in our short-term *in vitro* assays can translate *in vivo* (over much longer time scales associated with tumor progression) into significant reductions in overall accumulation of encapsulating collagen accompanied by increased abundance of linear fibers oriented perpendicularly to the tumor margin.

Discussion

Our results lead us to propose a novel mechanism by which tumor cells sense, respond to, and reorganize the ECM to support metastasis (summarized in Fig 7). Integrin-dependent outside-in signaling at FXs, as well as inside-out ECM remodeling are necessary for directional migration towards FN. FN and α5 expression are upregulated in breast cancer tumors and high levels of tumor FN and α5 have been associated with poor outcome(7), though not, by themselves, in the datasets we analyzed. Given the heterogeneous levels of FN within both the primary tumor and metastatic niche, disseminating cells must be able to migrate effectively through areas of different FN concentrations, as well as to move from areas of low FN to areas of high FN and vice versa. In addition to simply being permissive for migration, we show that FN acts as a directional cue *in vivo*. Expression of Mena drives haptotaxis at low FN concentrations, while expression of Mena^{INV} allows cells to migrate at high concentrations of FN similar to those present around blood vessels in tumors(9). Abrogation of the interaction between Mena/Mena^{INV} and α5β1 abolished haptotaxis *in vitro,* while also significantly decreasing metastasis in two mouse xenograft breast cancer models. Together, these findings support the idea that FN can act as a potent guidance and motility cue for tumor cells during metastatic progression.

At a mechanistic level, inclusion of the INV sequence increases the association of Mena with α5 by 2.2 fold. We propose that increased association of Mena^{INV} vs. Mena with α5 likely underlies the isoform-specific differences in α5β1-mediated effects on haptotaxis and focal complexes. The INV sequence is inserted between the amino terminal EVH1 domain in Mena, which mediates interactions with several other molecules associated with integrin function, and the LERER domain, which binds directly

to α5(15,36). It will be of great interest to determine exactly how the INV sequence modifies interactions with α5.

The ECM can also deliver signals to other types of receptors by providing binding sites for their ligands (37). While it is well established that proteoglycans directly bind growth factors, allowing the ECM to act as a reservoir for invasive signals (38), emerging evidence suggests that ECM proteins contain domains that may allow them to activate receptor tyrosine kinases directly. FN-mediated activation of α5β1 can, for example, lead to HGF-independent activation of Met to promote invasion in ovarian cancer cells (39). In addition, expression of mutant p53 protein, which is mutated in 50% of cancers (40), can drive invasion through enhanced RCP-dependent co-recycling of α5β1 with several receptor tyrosine kinases (RTKs), including EGFR and Met (25,41). Given that Mena^{INV} expression sensitizes cells to EGF, enabling them to invade and migrate in response to low EGF concentrations (17,18,42), it will be interesting to investigate the potential role of crosstalk with RTK signaling in Mena^{INV}-driven haptotaxis.

The importance of tumor-cell-driven FN fibrillogenesis and ECM remodeling in Mena^{INV}-driven haptotaxis is surprising. FN polymerization is required for deposition of collagen I(34) and antibody binding to the collagen-binding site on FN inhibits collagen fibrillogenesis(43). Here, we show for the first time that tumor-cell-mediated FN fibrillogenesis is required for haptotaxis, a process driven by expression of Mena^{INV}. We also show the first evidence for tumor-cell-driven collagen reorganization in vivo, also driven by Mena^{INV} and its interaction with α5β1. Together, these data suggest that tumor cells can pave their own way to blood vessels. While the mechanism by which FN and integrins drive collagen fibrillogenesis remains incompletely understood, our results indicate that Mena^{INV} provides a link between integrin activation and the cytoskeleton to drive ECM organization by tumor cells. The Mena^{INV}-driven reduction in collagen

encapsulation and increase in linear fibrils radiating from the tumor periphery, in turn, further enhance metastatic phenotypes. Overall, our findings highlight the potential importance of bi-directional integrin-mediated signaling in the tumor cell compartment in addition to the previously characterized contributions from stromal cells(4) in the regulation of ECM structure.

Our data also support a role for the relationship between Mena^{INV}, α5 and FN in human breast cancer. Using an isoform-specific antibody and bioinformatic analysis of available TCGA data, we found that high expression levels of Mena^{INV} and FN are associated with increased recurrence and poor outcome in two human breast cancer cohorts. Future studies on larger patient cohorts will be needed to help determine the utility of Mena^{INV} as a diagnostic and prognostic marker, and whether it provides additional information when used in conjunction with other tumor markers. Altogether, our findings reinforce the importance of Mena^{INV} in human breast cancer, and suggest that targeting the chemotactic and haptotatic pathways by which Mena^{INV} promotes invasion could be useful therapeutically for metastatic breast cancer.

Materials and methods

Antibody reagents, growth factors and inhibitors

Antibodies: α5 (for IF: BD Biosciences, #555651, for IP: Millipore, AB1928 and for WB: Santa Cruz Biotechnology, sc-166681), αv (BD Biosciences, 611012), α6 (Abcam, ab10566), α2 (Abcam, ab133557), β1 (BD Biosciences, 610467), FAK (BD Biosciences, 610087), pFAK Y397 (Invitrogen, 44-625G), Cleaved Caspase 3 (CST, 9661), Ki67 (CST, 9027), FN (BD Biosciences), p53 (CST, clone 1C12), RCP (Sigma). See (26) for description of Mena^{INV} rabbit monoclonal antibody. Animals were immunized with a peptide containing the sequence encoded by the INV exon. Clones were screened for Mena^{INV} specificity in Western blot assays and by immunostaining of FFPE tumor sections from wild type or Mena-null mice (FigS3) (26). Cilengitide (Selleck Chemicals), P1D6 α5 blocking antibody (DSHB), FAKi (Santa Cruz), 70kD fragment and its control peptide for blockade of fibrillogenesis (gift from Dr. Sottile, University of Rochester), FN 7-11, purified from a plasmid from ROH).

Cell culture

MDAMB231 cells were purchased directly from ATCC in June 2012, where cell lines are authenticated by short tandem repeat profiling. These cells not re-authenticated by our lab, and were cultured in DMEM with 10% FBS (Hyclone). SUM159 cells were obtained from Joan Brugge's lab at Harvard Medical School (January 2011) and were not re-authenticated in our lab. SUM159 cells were cultured according to the ATCC protocols. MV^{D7} fibroblasts cells were isolated from mice in our lab in October 1999 and cultured as previously described(15). These cell lines were authenticated in our lab and deletion of Mena was verified at the mRNA and protein level. Retroviral packaging, infection, and FACS were performed as previously described (15). Cell lines were engineered to

express Mena isoforms stably at 10-15-fold higher levels than parental lines. MV^{D7} fibroblasts were isolated were maintained at 32°C, 5% CO2 in DME supplemented with l-Glutamine, penicillin and streptomycin, 15% fetal bovine serum, and 50U/ml interferon (I-4777; Sigma) (15). Stable Knockdown cell lines were generated using mir30-based shRNA sequence 'CAGAAGACAATCGCCCTTTAA' for Mena expressing an mCherry tag.

Immunohistochemistry

Fixation, processing and staining of tissue sections from tumors was carried out as previously described (18). Tumors dissected from NOD/SCID mice were fixed in 10% buffered formalin and embedded in paraffin. Tissue sections (5μm thick) were deparaffinized followed by antigen retrieval using Citra Plus solution (Biogenex). After endogenous peroxidase inactivation, sections were incubated with primary antibodies overnight at 4°C and fluorescently labeled secondary antibodies at room temperature for 2 hrs. Sections were stained using the following antibodies: anti-Mena (1:500), anti-Ki67 (BD Biosciences), cleaved Caspase-3 (BD Biosciences). Fluorochromes on secondary antibodies included AlexaFluor 594, AlexaFluor488 and AlexaFluor 647 (Jackson Immunoresearch). Sections were mounted in Fluoromount mounting media and imaged at room temperature. Z series of images were taken on an Applied precision DeltaVision microscope using Softworx acquisition, an Olympus 40x 1.3 NA plan apo objective and a Photometrics CoolSNAP HQ camera. Images were deconvolved using Deltavision Softworx software and objective specific point spread function. At least 4 images were captured for each tumor, with at least 3 tumors per tumor group.

TMA

Details of the patient cohort and associated data used to generate the TMA are published (32). The TMA was stained by immunofluorescence and imaged with a Vectra automated slide scanner and a 20X objective. The field of view with this objective covers 90% of the core spot. Each patient had three cores on the TMA. All were imaged, but some had to removed due to lack of tissue or folded tissue. Fluorescence intensity in the tumor compartment was analyzed using Inform software. Mena^{INV} and FN intensity metrics are in arbitrary units.

Haptotaxis assays

Microfluidic devices were prepared as described (19). For haptotaxis on a 2D matrix, after bonding PDMS devices to Mattek dishes, the chamber was coated with 0.1mg/ml Collagen I for 1hr at 37°C and then 250μg/ml fluorescently-labeled FN was flowed through the source channel for 1hr. Cells were then plated in the device in full serum media and left to attach for 1hr before imaging. For haptotaxis in a 3D matrix, cells were resuspended in 1mg/ml collagen I (BD Biosciences) with 10X DMEM and 1N NaOH and 3nM EGF in full serum media, plated in the cell culture chamber, and left to settle for 8hrs at 37°C. Fluorescently-labeled FN was then flowed through the source channel for 1hr before imaging. For all haptotaxis experiments, the FN concentration represents the concentration at the top of the gradient. Unless mentioned, FN concentration at the top of the gradient is 125μg/ml. Cells were imaged overnight in the haptotaxis device, with images being acquired every 10min for 16hr in an environmentally controlled microscope (TE2000, Nikon) with a 20X objective and a Photometrics Coolsnap HQ camera. Individual cells were manually tracked using ImageJ software Manual Tracking plug-in. The tracks obtained were analyzed using the Chemotaxis Tool ImageJ plugin (from Ibidi). This analysis tool was used to extract the FMI (Fig 1A) along with the velocity of

migration and the persistence of migration using the D/T ratio (net path length/total path length) (20,44).

Tumor formation and metastasis assay

All animal experiments were approved by the MIT Division of Comparative Medicine. For xenograft experiments, MDAMB231 or SUM159 cells (2 million per mouse in PBS and 20% collagen I) expressing different Mena isoforms were injected into the 4th right mammary fat pad of six week-old female NOD-SCID mice (Taconic). Tumor size was measured weekly with calipers. 8 or 12 weeks post-surgery, once tumors had reached 1cm in diameter, mice were used for intravital imaging, and then sacrificed and their tumors and lungs were fixed in 4% formalin overnight. Metastatic index was calculated by counting the number of metastases in each lobe relative to the weight of the tumor. Each tumor group contained 4-6 mice. PyMT-MMTV mice were obtained from Jackson, mice were left to growth for 15-20 weeks, when they had developed tumors of about 1.5 cm in diameter. Histological analysis of H&Es from these tumors confirmed these tumors were advanced carcinoma.

***In vivo* invasion assay**

The *in vivo* invasion assay was performed in at least 4 mice per condition as previously described (45). Briefly, needles were held in place by a micromanipulator around a single mammary tumor of an anesthetized mouse. Needles contained a mixture of 0.5mg/ml Collagen I, EDTA with L-15 media or increasing amounts with FN. After four hours, the contents of the needles were extruded. Cells were stained with DAPI and counted.

Intravital Imaging and *in vivo* haptotaxis

Intravital multiphoton imaging was performed as described previously (23) using a 25x 1.05NA water immersion objective with correction lens. For *in vivo* haptotaxis, a microscale device filled with multiple reservoirs(28) with powdered rhodamine-FN or dextran was prepared. After exposing the tumor, the device was implanted into the tumor edge. Hour-long time-lapse movies were analyzed for frequency of motility and tracking, and to measure and quantify cell characteristics in 3D and over time using NIH ImageJ. Cells that were either protruding or moving were counted as motile. For each movie, the FMI was calculated, with the angle for each track made relative to the direction of FN gradient for each frame. Data is pooled from 2-4 mice per tumor group, with 4-10 fields imaged per mouse, with a total of at least 70 cells per tumor type tracked. Collagen signal was visualized by second harmonic generation and images were analyzed using CT-Fire software (46) to calculate collagen fiber orientation, width and length. Data were pooled from 2-4 mice per tumor group, with 4-10 fields imaged per mouse.

Western Blot/Immunoprecipitation

For the α5 immunoprecipitation, 231-Mena and 231-Mena^{INV} were lysed with CSK buffer (10 mM PIPES – pH 6.8, 50 mM NaCl, 150 mM sucrose, 3 mM $MgCl_2$, 1 mM $MnCl_2$, 0.5% Triton X-10, protease and phosphatase inhibitors) and passed through a 23-gauge needle. Lysates were precleared with protein A beads for 1.5 h, incubated with the integrin α5 antibody (1928; Millipore) for 2.5 h at 4°C, and then captured with 3% BSA-blocked protein A beads for 2 h. Beads were washed three times in CSK lysis buffer, and proteins were eluted in 2x sample buffer. Standard procedures were used for protein electrophoresis, western blotting, and immunoprecipitation. MDAMB231 expressing different Mena isoforms were lysed in 25mM Tris, 150mM NaCl, 10% glycerol, 1% NP

40 and 0.5M EDTA with a protease Mini-complete protease inhibitors (Roche) and a phosphatase inhibitor cocktail (PhosSTOP, Roche) at 4°C. Protein lysates were separated by SDS-PAGE, transferred to a nitrocellulose membrane, blocked with Odyssey Blocking Buffer (LiCor), incubated in primary antibody overnight at 4°C. Proteins were detected using Licor secondary antibodies. Protein level intensity was measured with Image J and data were pooled from at least 3 different experiments.

FACs

MDAMB231 cells expressing the different isoforms were trypsinized, resuspended in media, and then incubated with a primary antibody in PBS and 5% media for 30mins on ice. Next, the cells were incubated with a species appropriate Alexa647-tagged secondary antibody and then resuspended in PBS with 10μg/ml propidium iodide. Samples were then analyzed on a FACS-Calibur machine (BD Biosciences). Data is pooled from at least 3 separate experiments, with 10 000 cells analyzed per experiment.

Immunofluorescence

Cells were plated in a haptotaxis device on a 125 μg/ml 2D FN gradient for 3 hr or on collagen-coated glass-bottomed dishes (MatTek) in serum-free media for 30 min at 37°C. Cells were then fixed for 20 min in 4% paraformaldehyde in PHEM buffer, then permeabilized with 0.2% TritonX-100, blocked with 10% BSA and incubated with primary antibodies overnight at 37°C. Z series of images were taken on an Applied Precision DeltaVision microscope using Softworx acquisition, an Olympus 40x 1.3 NA plan apo objective and a Photometrics CoolSNAP HQ camera. Images were deconvolved using Deltavision Softworx software and objective specific point spread function. Images were analyzed with ImageJ. Images are pooled from at least 3 independent experiments, at

least 10 cells per experiment.

Mena^{INV} TCGA data retrieval

RNAseq data in fastq format were obtained from TCGA. For each sample, ENAH (Mena)-derived reads were extracted from the full dataset by aligning to a target database that contained collection of all possible ENAH isoforms using BWA version 0.7.10. Properly paired ENAH reads were then extracted with Samtools version 0.1.19. ENAH isoforms were then quantified by aligning to hg19 using tophat2 version 2.0.12 guided with an edited GTF file derived from the USCS known genes annotation that contained all ENAH variants of interest. Bedtools version 2.20.1 and a custom python script were then used to count reads that overlap with each ENAH exon. The resulting counts per exon were then normalized for RNA loading by calculating a counts per million reads per Kb of mRNA using a sum of exon-level counts in the publicly available and preprocessed TCGA data as the total aligned counts denominator.

Survival/recurrence data analysis

The relationship between Mena/Mena^{INV} expression levels (from mRNA TCGA or protein TMA) and survival (time to death) or metastasis (time to recurrence) was assessed by Log rank Mantel-Cox test. In each samples, patients were binned into quartiles according Mena or Mena^{INV} expression (Q1 being the highest level of expression and Q4 being the lowest). The hazard ratio for each quartile (with 95% confidence interval values) was calculated. The p value generated by this log rank test evaluates whether the difference in the curves is significantly different. We also performed the Log rank test for trend to further assess the differences between the curves representing patients with varying levels of Mena isoform expression.

The hazard effects of Mena^{INV} and Mena upon the time to death were investigated by Cox regression using R 2.15.3 basing on TCGA BRCA data. In order to make comparison across variables, we first standardized Mena and Mena^{INV} RPKM values to mean zero and standard deviation one. Cox regressions were then carried out basing on the standardized Mena^{INV} values or the standardized Mena RPKM values as the only independent variable to predict the effects upon the time of death of the BRCA patients in TCGA study. The association between Menal^{NV}/Mena expression level and survival status of TCGA BRCA subjects was evaluated by logistic regression using R 2.15.3. In order to compare coefficients across tests, we first standardized INV and Mena values to be mean zero and standard deviation one. Logistic regressions were conducted by choosing survival status as dependent variable (1 as death, and 0 as alive). The only independent variable fitted in the model was INV, or Mena respectively. P values and coefficients corresponding to the independent variables were used to judge the significance of the association as well as the strength of the association.

Author contributions:

MJO designed and performed experiments, data analysis and prepared the manuscript. FBG guided overall experimental design, performed TCGA data analysis and helped prepare the manuscript. OJ developed the microscale device and helped design *in vivo* haptotaxis experiments, TK and LCB performed haptotaxis assays, immunofluorescence, western blots, BCG performed the Mena-α5 IP experiments, JW assisted with intravital imaging and intravital imaging, DR developed and validated the shMena constructs, JML helped with animal experiments, SBA helped with *in vitro* haptotaxis assays. CW and DM performed TCGA data retrieval and analysis. KBW generated the TMA. RL, MJC, JEB, DAL, PK, ROH and FBG were involved in the study design and data interpretation. All authors discussed the results and commented on the manuscript.

Acknowledgements:

We thank the Microscopy, Flow Cytometry and Histology facilities in the KI Swanson Biotechnology Center for support. We thank MetaStat for use of a Vectra scanner and software. We thank Jenny Tadros for help with cell line generation, Shannon Hughes for the cloning of Mena shRNA constructs, and Jane Sottile (Rochester) for the 70kD FN fragment.

References

1. Joyce JA, Pollard JW. Microenvironmental regulation of metastasis. Nat Rev Cancer, 2009;9:239–52.
2. Pickup MW, Mouw JK, Weaver VM. The extracellular matrix modulates the hallmarks of cancer. EMBO Rep. EMBO Press; 2014;15:1243–53.
3. Naba A, Clauser KR, Lamar JM, Carr SA, Hynes RO. Extracellular matrix signatures of human mammary carcinoma identify novel metastasis promoters. Elife. 2014; 3:e01308.
4. Conklin MW, Keely PJ. Why the stroma matters in breast cancer: insights into breast cancer patient outcomes through the examination of stromal biomarkers. Cell Adh Migr; 2012;6:249–60.
5. Conklin MW, Eickhoff JC, Riching KM, Pehlke CA, Eliceiri KW, Provenzano PP, et al. Aligned collagen is a prognostic signature for survival in human breast carcinoma. Am J Pathol; 2011;178:1221–32.
6. Ioachim E, Charchanti A, Briasoulis E, Karavasilis V, Tsanou H, Arvanitis DL, et al. Immunohistochemical expression of extracellular matrix components tenascin, fibronectin, collagen type IV and laminin in breast cancer: Their prognostic value and role in tumour invasion and progression. Eur J Cancer. 2002;38:2362–70.
7. Bae YK, Kim A, Kim MK, Choi JE, Kang SH, Lee SJ. Fibronectin expression in carcinoma cells correlates with tumor aggressiveness and poor clinical outcome in patients with invasive breast cancer. Hum Pathol. 2013;44:2028–37.
8. Roussos ET, Condeelis JS, Patsialou A. Chemotaxis in cancer. Nat Rev Cancer; 2011;11:573–87.
9. Astrof S, Crowley D, George EL, Fukuda T, Sekiguchi K, Hanahan D, et al. Direct test of potential roles of EIIIA and EIIIB alternatively spliced segments of fibronectin in physiological and tumor angiogenesis. Mol Cell Biol. 2004;24:8662–70.
10. Levental KR, Yu H, Kass L, Lakins JN, Egeblad M, Erler JT, et al. Matrix Crosslinking Forces Tumor Progression by Enhancing Integrin Signaling. Cell. 2009;139:891–906.
11. Huttenlocher A, Horwitz AR. Integrins in cell migration. Cold Spring Harb Perspect Biol. 2011;3:1–16.
12. Schwarzbauer JE, DeSimone DW. Fibronectins, their fibrillogenesis, and in vivo functions. Cold Spring Harb. Perspect. Biol. 2011; 3:1–19.
13. Kadler KE, Hill A, Canty-Laird EG. Collagen fibrillogenesis: fibronectin, integrins, and minor collagens as organizers and nucleators. Curr. Opin. Cell Biol. 2008; 20: 495–501.
14. Gertler F, Condeelis J. Metastasis: tumor cells becoming MENAcing. Trends Cell Biol. 2011;21:81–90.
15. Gupton SL, Riquelme D, Hughes-Alford SK, Tadros J, Rudina SS, Hynes RO, et al. Mena binds α5 integrin directly and modulates α5β1 function. J Cell Biol; 2012;198:657–76.
16. Goswami S, Philippar U, Sun D, Patsialou A, Avraham J, Wang W, et al. Identification of invasion specific splice variants of the cytoskeletal protein Mena

present in mammary tumor cells during invasion in vivo. Clin Exp Metastasis; 2009;26:153–9.

17. Philippar U, Roussos ET, Oser M, Yamaguchi H, Kim H-D, Giampieri S, et al. A Mena Invasion Isoform Potentiates EGF-Induced Carcinoma Cell Invasion and Metastasis. Dev Cell; 2008;15:813–28.
18. Roussos ET, Balsamo M, Alford SK, Wyckoff JB, Gligorijevic B, Wang Y, et al. Mena invasive (MenaINV) promotes multicellular streaming motility and transendothelial migration in a mouse model of breast cancer. J Cell Sci; 2011;124:2120–31.
19. Wu C, Asokan SB, Berginski ME, Haynes EM, Sharpless NE, Griffith JD, et al. Arp2/3 is critical for lamellipodia and response to extracellular matrix cues but is dispensable for chemotaxis. Cell. 2012;148:973–87.
20. Asokan SB, Johnson HE, Rahman A, King SJ, Rotty JD, Lebedeva IP, et al. Mesenchymal Chemotaxis Requires Selective Inactivation of Myosin II at the Leading Edge via a Noncanonical PLCγ/PKCα Pathway. Dev Cell; 2014;31:747–60.
21. Bear JE, Loureiro JJ, Libova II, Fässler RR, Wehland JJ, Gertler FBFB. Negative regulation of fibroblast motility by Ena/VASP proteins. Cell; 2000;101:717–28.
22. Leyme A, Marivin A, Perez-Gutierrez L, Nguyen LT, Garcia-Marcos M. Integrins activate trimeric G proteins via the nonreceptor protein GIV/Girdin. J Cell Biol. 2015;210:1165–84.
23. Wang W, Goswami S, Lapidus K, Wells AL, Wyckoff JB, Sahai E, et al. Identification and testing of a gene expression signature of invasive carcinoma cells within primary mammary tumors. Cancer Res. 2004;64:8585–94.
24. Hynes RO, Yamada KM. Fibronectins: Multifunctional modular glycoproteins. J. Cell Biol. 1982;95:369–77.
25. Muller PAJ, Caswell PT, Doyle B, Iwanicki MP, Tan EH, Karim S, et al. Mutant p53 Drives Invasion by Promoting Integrin Recycling. Cell. 2009;139:1327–41.
26. Oudin MJ, Hughes SK, Rohani N, Moufarrej MN, Jones JG, Condeelis JS, et al. Characterization of the expression of the pro-metastatic Mena(INV) isoform during breast tumor progression. Clin Exp Metastasis. 2015, Dec 17, Epub ahead of print
27. Wyckoff JB, Segall JE, Condeelis JS. The collection of the motile population of cells from a living tumor. Cancer Res; 2000;60:5401-4.
28. Jonas O, Landry HM, Fuller JE, Santini JT, Baselga J, Tepper RI, et al. An implantable microdevice to perform high-throughput in vivo drug sensitivity testing in tumors. Sci Transl Med. 2015;7:284ra57.
29. Pignatelli J, Goswami S, Jones JG, Rohan TE, Pieri E, Chen X, et al. Invasive breast carcinoma cells from patients exhibit MenaINV- and macrophage-dependent transendothelial migration. Sci Signal. 2014;7:ra112.
30. Cancer Genome Atlas Network. Comprehensive molecular portraits of human breast tumours. Nature; 2012;490:61–70.
31. Lin EY, Jones JG, Li P, Zhu L, Whitney KD, Muller WJ, et al. Progression to malignancy in the polyoma middle T oncoprotein mouse breast cancer model provides a reliable model for human diseases. Am J Pathol; 2003;163:2113–26.

32. Wang L, Zhao Z, Meyer M, Saha S, Yu M, Guo A, et al. CARM1 methylates chromatin remodeling factor BAF155 to enhance tumor progression and metastasis. Cancer Cell. 2014;25:21–36.

33. Hynes RO. Integrins: Bidirectional, allosteric signaling machines. Cell. 2002; 110: 673–87.

34. Sottile J, Hocking DC. Fibronectin polymerization regulates the composition and stability of extracellular matrix fibrils and cell-matrix adhesions. Mol Biol Cell. 2002;13:3546–59.

35. Roussos ET, Wang Y, Wyckoff JB, Sellers RS, Wang W, Li J, et al. Mena deficiency delays tumor progression and decreases metastasis in polyoma middle-T transgenic mouse mammary tumors. Breast Cancer Res; 2010;12:R101.

36. Gertler F, Condeelis J. Metastasis: tumor cells becoming MENAcing. Trends Cell Biol. 2011;21:81–90.

37. Hynes RO. The extracellular matrix: not just pretty fibrils. Science; 2009;326:1216–9.

38. Iyer AK V, Tran KT, Griffith L, Wells A. Cell surface restriction of EGFR by a tenascin cytotactin-encoded EGF-like repeat is preferential for motility-related signaling. J Cell Physiol. 2008;214:504–12.

39. Mitra AK, Sawada K, Tiwari P, Mui K, Gwin K, Lengyel E. Ligand-independent activation of c-Met by fibronectin and α(5)β(1)-integrin regulates ovarian cancer invasion and metastasis. Oncogene. 2011;30:1566–76.

40. Vogelstein B, Lane D, Levine AJ. Surfing the p53 network. Nature. 2000; 408:307–10.

41. Muller PAJ, Trinidad AG, Timpson P, Morton JP, Zanivan S, van den Berghe PVE, et al. Mutant p53 enhances MET trafficking and signalling to drive cell scattering and invasion. Oncogene. 2013; 32:1252-65.

42. Hughes SK, Oudin MJ, Tadros J, Neil J, Del Rosario A, Joughin BA, et al. PTP1B-dependent regulation of receptor tyrosine kinase signaling by the actin-binding protein Mena. Mol Biol Cell. 2015; 26:3867-78.

43. McDonald JA, Kelley DG, Broekelmann TJ. Role of fibronectin in collagen deposition: Fab' to the gelatin-binding domain of fibronectin inhibits both fibronectin and collagen organization in fibroblast extracellular matrix. J Cell Biol. 1982;92:485–92.

44. Chan KT, Asokan SB, King SJ, Bo T, Dubose ES, Liu W, et al. LKB1 loss in melanoma disrupts directional migration toward extracellular matrix cues. J Cell Biol. 2014;207:299–315.

45. Wyckoff J. A Paracrine Loop between Tumor Cells and Macrophages Is Required for Tumor Cell Migration in Mammary Tumors. Cancer Res. 2004;64:7022–9.

46. Bredfeldt JS, Liu Y, Pehlke C a, Conklin MW, Szulczewski JM, Inman DR, et al. Computational segmentation of collagen fibers from second-harmonic generation images of breast cancer. J Biomed Opt. 2014;19:16007.

Figure legends

Figure 1: Mena-driven haptotaxis *in vitro* on FN gradients in 2D and 3D is dependent upon its direct interaction with α5 integrin and F-actin. A) Schematic diagram of a microfluidic device used for 2D or 3D haptotaxis, representative image of a FN gradient in a collagen gel, and a diagram describing the FMI used to quantify haptotaxis. B) Expression of Mena, but not VASP or EVL, in MV^{D7} fibroblasts drives haptotaxis on a 2D FN gradient (125μg/ml at top of gradient), as measured by the FMI. C) 231-Mena cells haptotax when plated on a 2D FN gradient (125μg/ml at top of gradient), but not on a LN or VN gradient, as measured by the FMI. D) MDAMB231 cells 231-Mena cells plated in a 3D collagen gel and subjected to increasing concentrations of FN at the top of the gradient. E) Inhibition of α5β1 with P1D6 (0.5μg/ml) blocked Mena-driven haptotaxis in 3D collagen gels, as measured by FMI, while inhibition of αvβ3 with Cilengitide (1μM) had no effect. F) Diagram of structure of Mena and its domains, including the LERER domain and the F-Actin binding domain (FAB). Deletion of the LERER domain abrogates the interaction of Mena/$Mena^{INV}$ with α5. G) 231-MenaΔLERER and MenaΔFAB cells did not haptotax in 3D collagen gels and this effect was independent of an effect on velocity (μm/min) (H). For each experiment, n=3 experiments, at least 80 cells tracked per condition. Results show mean ± SEM, significance by one way ANOVA, *p<0.5, **p<0.01, ***p<0.005. See FigS1.

Figure 2: $Mena^{INV}$-drives haptotaxis at high FN concentrations *in vivo* and *in vitro* A) 231-$Mena^{INV}$ cells plated in a 3D collagen gel and subjected to increasing concentrations of FN at the top of the gradient B) Inhibition of α5 with P1D6 (0.5μg/ml) blocked $Mena^{INV}$-driven 3D haptotaxis, as measured by FMI, while inhibition of αvβ3 with Cilengitide had no effect. 231-$Mena^{INV}$ΔLERER or 231-$Mena^{INV}$ΔFAB did not haptotax in

3D. (n=3 experiments, ≥150 cells tracked per condition). C) *In vivo* invasion assay into needles inserted in tumors generated in NOD/SCID mice with MDAMB231 cells expressing Control-GFP, Mena or Mena^{INV}. Needles contained 0.5mg/ml collagen and increasing amounts of FN (n=4 mice per condition). Results show mean ± SEM. Stars above columns represent significance relative to collagen only by one-way ANOVA. D) Representative image of a FN gradient (Rhodamine-labeled FN, shown in red) on collagen fibers (shown in white) generated using a microscale implantable device implanted into the tumor (tumor cells labeled with GFP shown in green) and visualized by intravital imaging. Scale bar is 100μm. FMI of E) MDAMB231 and F) SUM159 tumor cells expressing different Mena isoforms in the absence of a device, or in the presence of a device releasing fluorescently labeled FN or similarly sized Dextran (data pooled ≥8 movies from ≥2 mice per condition). Results show mean ± SEM, significance by one way ANOVA, *p<0.5, **p<0.01, ***p<0.005. See FigS2.

Figure 3: Mena^{INV} is associated with poor outcome in human tumors and requires its interaction with α5 integrin for metastasis

Kaplan-Meier curves for survival of breast cancer patients binned by quartiles of Mena (A) or Mena^{INV} (B) mRNA levels, as indicated (Q1 had the highest expression, Q4 the lowest). Data are from 128 breast cancer cases with >10 years of follow up BRCA TCGA dataset (data from entire 1060 patient cohort in Figs S3A-D). Significance calculated by log-rank Mantel-Cox test, hazard ratio calculated by logrank test, p_{Trend} calculated by log-rank test for Trend (see methods). C) COX regression carried out to assess the relationship between Mena or Mena^{INV} and time to death in breast cancer patients (patients with 10-year follow-up). D) Logistic regression carried out to assess the relationship between Mena or Mena^{INV} and survival in breast cancer patients (patients with 10-year follow-up). E) Representative images of PyMT-MMTV tumors stained for

Mena (red) and Mena^{INV} (green) Scale bar = 20μm. F) Representative images of PyMT-MMTV stained for Mena^{INV} (green) and integrin α5 (red) Same scale as E. G) Representative image from a wild-type PyMT tumor FN (red), Mena^{INV} (green) and nuclei (DAPI staining) Scale bar = 100μm. H) Correlation between Mena^{INV} and collagen FN intensity. Data from over 50 fields from 4 PyMT mice, each dot represents an individual field. I) Representative image of tumor spot from a tissue microarray with high levels of Mena^{INV} (green) and FN (red). J) Correlation between FN and Mena^{INV} staining in the entire patient cohort. K) Mena^{INV} expression in 300 breast cancer patients comparing patients with or without recurrence, data shows mean +/- SEM. L) Table showing the median recurrence-free time in months and corresponding p-value in patients with high vs. low Mena^{INV}, high vs., low FN or high vs. low Mena^{INV}+FN. Significance calculated by log-rank Mantel-Cox test. M) Representative fluorescence images of GFP-positive metastasis in lungs of mice with 231-Control, Mena or Mena^{INV} tumors. Scale bar = 50μm. N) H&E images of FFPE sections cut from the lungs of mice bearing MDAMB231 tumors expressing different Mena isoforms. Scale bar is 100μm**.** O) Lung metastatic index of NOD-SCID mice bearing tumors grown from MDAMB231 cells expressing different GFP-tagged Mena isoforms and measuring at least 1 cm in diameter (n≥4 mice per cell line). Data show mean ± SEM, significance by one way ANOVA, *p<0.5, **p<0.01, ***p<0.005. See FigS3 and S4.

Figure 4: Mena^{INV} drives haptotaxis via increased FX signaling A) Representative images of 231-Control, Mena and Mena^{INV} cells plated on FN and collagen, stained with antibodies to α5, and GFP (to visualize tagged GFP-Mena or GFP- Mena^{INV}) and with phalloidin to visualize F-actin. Scale bar = 5μm. B) Magnification of inset shown in (A). Scale bar = 1μm. C) Quantification of cell area (in μm^2) of MDAMB231 cells expressing different isoforms when plated on collagen (0.1mg/ml) + FN (50μg/ml). D) Number of α5-

positive adhesions relative to cell area for 231-Mena and 231-Mena^{INV} cells for cells plated on collagen only, collagen (0.1mg/ml) + FN (50μg/ml), and in the presence of P1D6, α5-function blocking antibody. E) Number of α5-positive adhesions relative to cell area for cells plated on collagen + FN. F) Intensity of α5 signal in Mena-positive adhesions (as counted by GFP positivity) for 231-Mena and 231-Mena^{INV} cells plated on collagen only, collagen (0.1mg/ml) + FN (50μg/ml), and in the presence of P1D6, α5-function blocking antibody. G) Intensity of α5 signal in Mena-positive adhesions (as counted by GFP positivity) in cells plated on a low 2D 125 μg/ml FN gradient. H) Inhibition of FAK (0.5μM) decreased Mena^{INV}-driven 2D haptotaxis on a low 2D 125 μg/ml FN gradient. Data from ≥3 experiments, with ≥80 cells tracked per condition. I) Representative images of 231-Control, Mena and Mena^{INV}, 231-MenaΔLERER and MenaΔFAB cells plated on a low 2D 125 μg/ml FN gradient, stained with pFAK397 (red) and Phalloidin to visualized F-actin (blue). Scale bar = 5μm. J) Quantification of pFAK Y397-positive adhesions in 231-Control, Mena or Mena^{INV}, while plated on a 2D low 125 μg/ml FN gradient K) 231-Mena^{INV}ΔLERER or 231-Mena^{INV}ΔFAB cells had decreased number of pFAK Y397-positive adhesions on a 2D low 125 μg/ml FN gradient. L) Quantification of pFAK Y397-positive adhesions in 231-Control, Mena or Mena^{INV}, while plated on a 2D high 500 μg/ml FN gradient Data pooled from 3 experiments, with at least 30 cells analyzed per condition. M) Representative image of a WB for α5-immunoprecipitation from 231-Mena and 231-Mena^{INV} lysates, probed for Mena, α5 and Tubulin. N) Quantification of fold increase in Mena pulled down in α5-IP, n=4. For all staining experiments, data pooled from at least 3 experiments, with at least 10 cells analyzed per experiments. Results show mean ± SEM, significance by one way ANOVA, *p<0.5, **p<0.01, ***p<0.005. Stars above data set represent significance relative to control. See FigS5.

Figure 5: Mena^{INV}-dependent directional motility requires ECM reorganization *in vitro* A) Representative images of MDAMB231 cells (outlined in white) and 231-Mena^{INV} cells (green) in a 3D 125μg/ml FN gradient (red) in a collagen gel (blue) in merged image; middle and right panels show grayscale images of FN and Collagen alone, respectively. Scale bar is 25μm**.** 231-Mena^{INV} showed increased accumulation and reorganization of B) FN and C) Collagen, in both low 125μg/ml and high 500μg/ml 3D FN gradients. D) A gradient of recombinant 7-11 domains of FN failed to induce 3D haptotaxis of 231-Mena^{INV} cells, as measured by the FMI E) Inhibition of FN fibrillogenesis by inclusion of a 70kD fragment ablated Mena^{INV} –dependent haptotaxis in 3D FN gradients (n=3 experiments, ≥80 cells tracked per condition). Deletion of the FAB and LERER regions in Mena^{INV}, and inhibition of α5β1 with P1D6, but not Cilengitide, reduced collagen (F) and collagen (G) accumulation at low FN concentrations. Data from ≥3 experiments, with ≥30 cells analyzed per condition. Results show mean ± SEM, significance by one way ANOVA, *p<0.5, **p<0.01, ***p<0.005. See FigS6.

Figure 6: Mena^{INV} drives collagen reorganization in tumors. A) Representative image from a wild type and Mena -/- PyMT tumor showing collagen as imaged by SHG (gray) and nuclei (DAPI staining). Scale bar = 100μm. B) Quantification of collagen signal as measured by SHG signal in wild type and Mena -/- PyMT tumors. Data from over 30 fields from 4 mice for wild-type mice and 2 mice for Mena -/-, each dot represents an individual field. C) Representative image from a wild-type PyMT tumor showing collagen as imaged by SHG (gray) and Mena^{INV} (green). Scale bar = 100μm. D) Correlation between Mena^{INV} and collagen intensity. Data from over 50 fields from 4 mice, each dot represents an individual field. E) Representative images showing collagen by SHG from a breast cancer patient samples with high or low Mena^{INV}. F) Collagen intensity in 30 patients with high or low Mena^{INV} expression. G) Representative images of collagen

organization (gray) of 231-Control, Mena and Mena^{INV} xenograft tumors taken by intravital imaging. Scale bar is 100μm. H) Representative diagram of angle used to measure the orientation of individual collagen fibers relative to the edge of the tumors. Plotted distributions of collagen fiber orientation relative to tumors edge comparing Control, Mena and Mena^{INV} expressing H1) MDAMB231 and H2) SUM159 cells. Data pooled from ≥15 images from ≥4 mice per condition. Results show mean ± SEM, significance by t-test, *p<0.5, **p<0.01, ***p<0.005. See Fig S6

Figure 7: Summary diagram: FN levels are high around blood vessels and at invasive edges in tumors. Expression of Mena in tumor cells allows cells to haptotax on low gradients of FN, via its weak association with α5 and increased FX signaling. Expression of Mena^{INV} allows cells to haptotax on both low and high FN gradients via increased association with α5, leading to increased FX number and FAK signaling at FXs, as well as through ECM reorganization.

Author Manuscript Published OnlineFirst on January 25, 2016; DOI: 10.1158/2159-8290.CD-15-1183
Author manuscripts have been peer reviewed and accepted for publication but have not yet been edited.

Figure 1

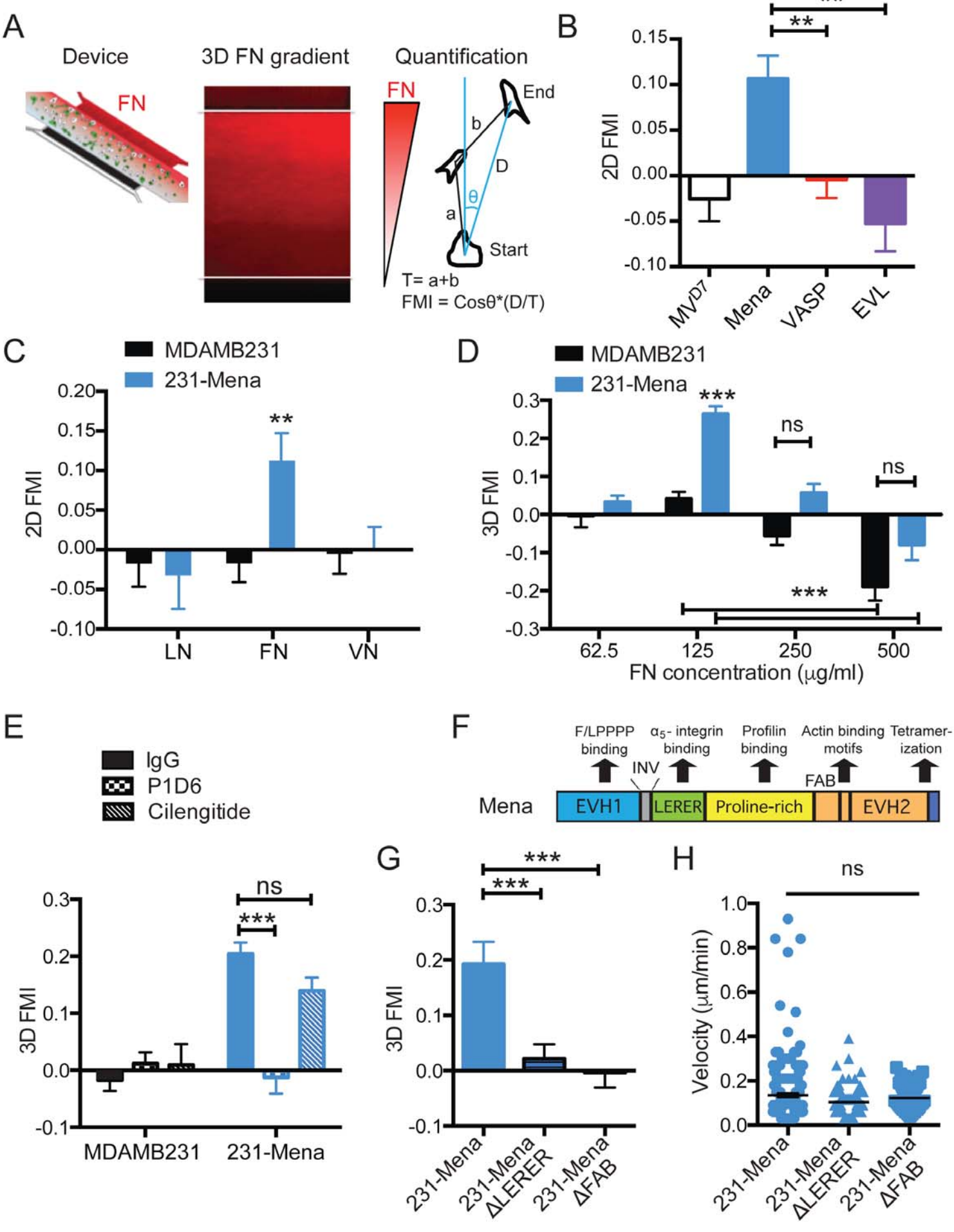

Author Manuscript Published OnlineFirst on January 25, 2016; DOI: 10.1158/2159-8290.CD-15-1183
Author manuscripts have been peer reviewed and accepted for publication but have not yet been edited.

Figure 2

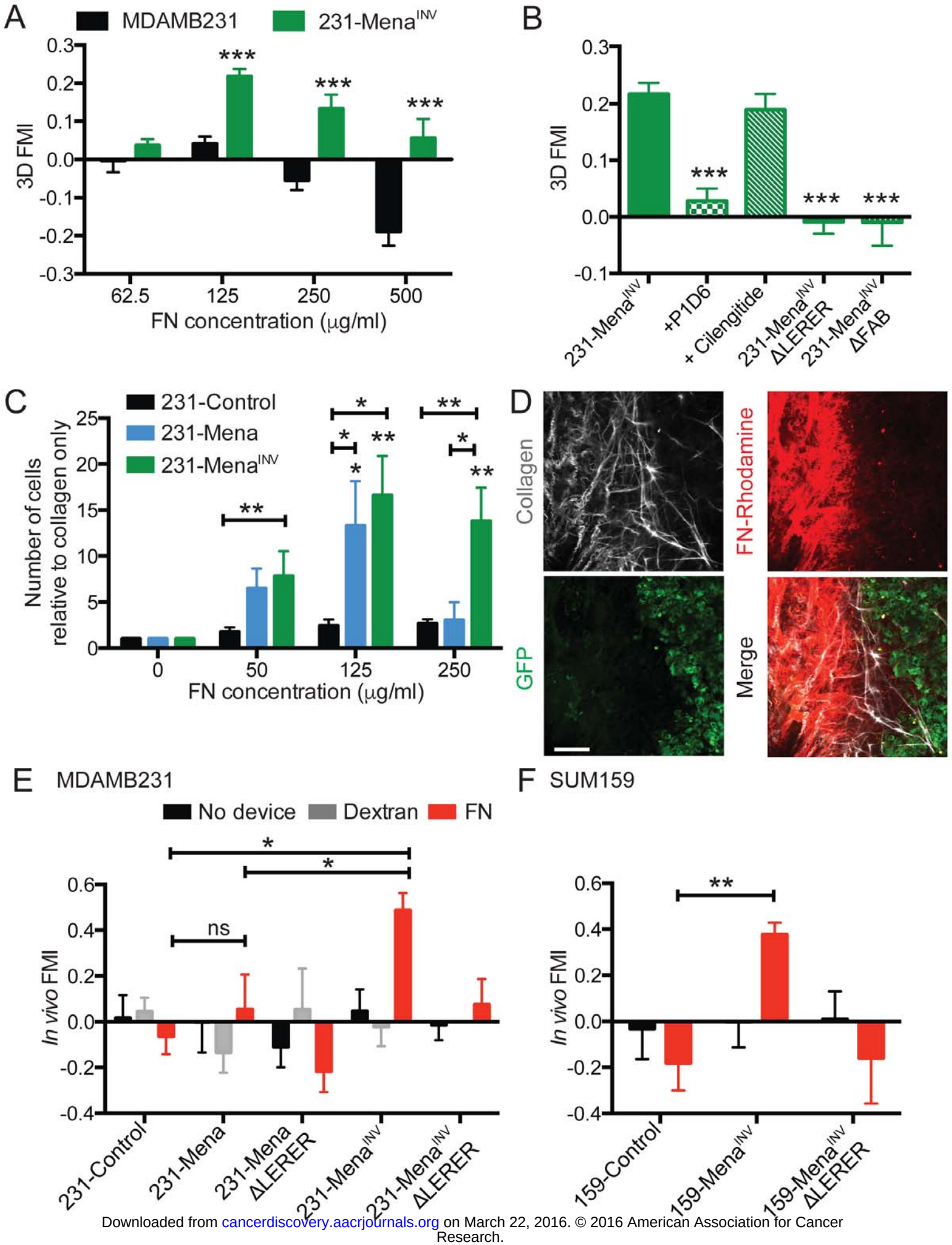

Author Manuscript Published OnlineFirst on January 25, 2016; DOI: 10.1158/2159-8290.CD-15-1183
Author manuscripts have been peer reviewed and accepted for publication but have not yet been edited.

Figure 3

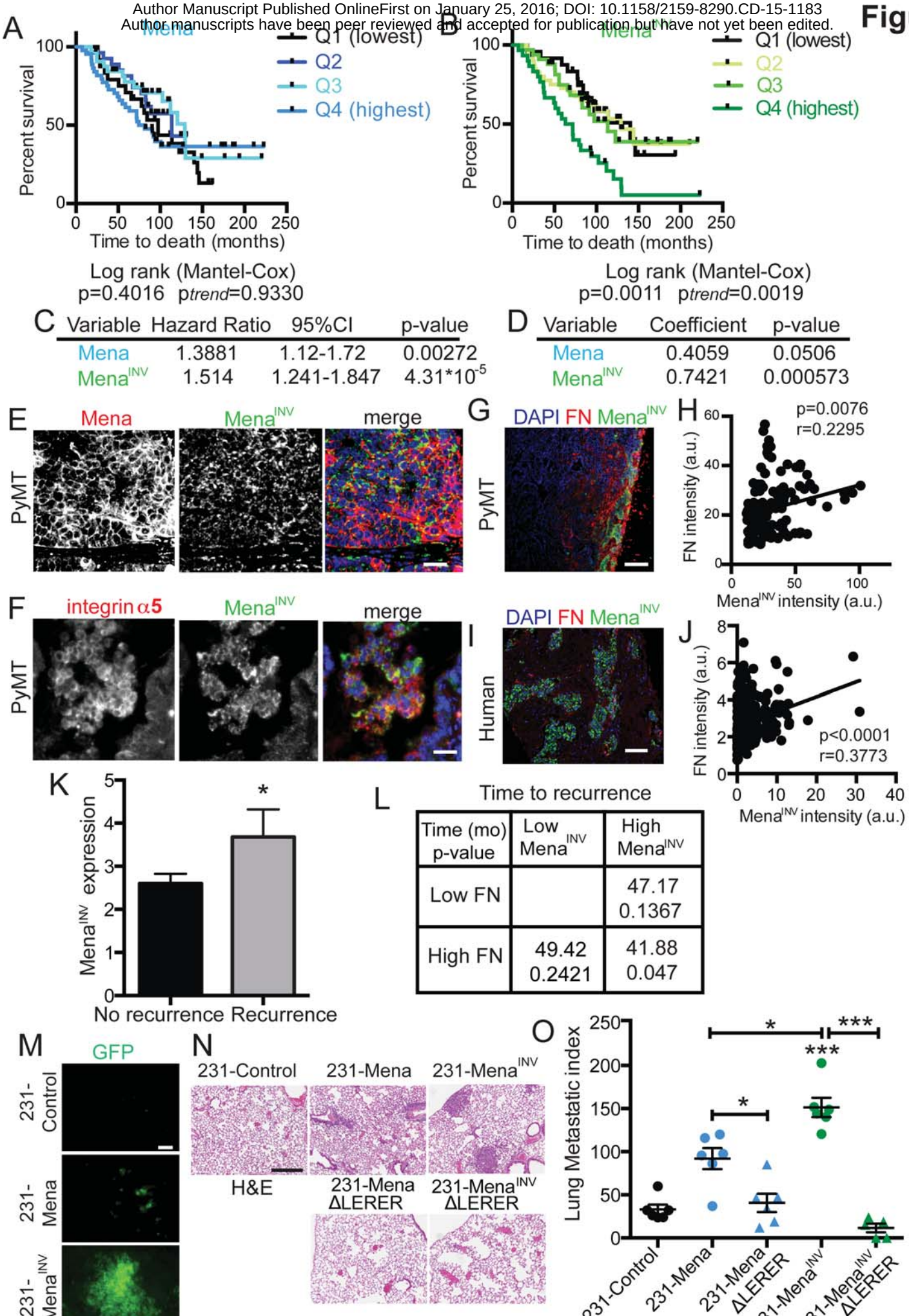

Author Manuscript Published OnlineFirst on January 25, 2016; DOI: 10.1158/2159-8290.CD-15-1183
Author manuscripts have been peer reviewed and accepted for publication but have not yet been edited.

Figure 4

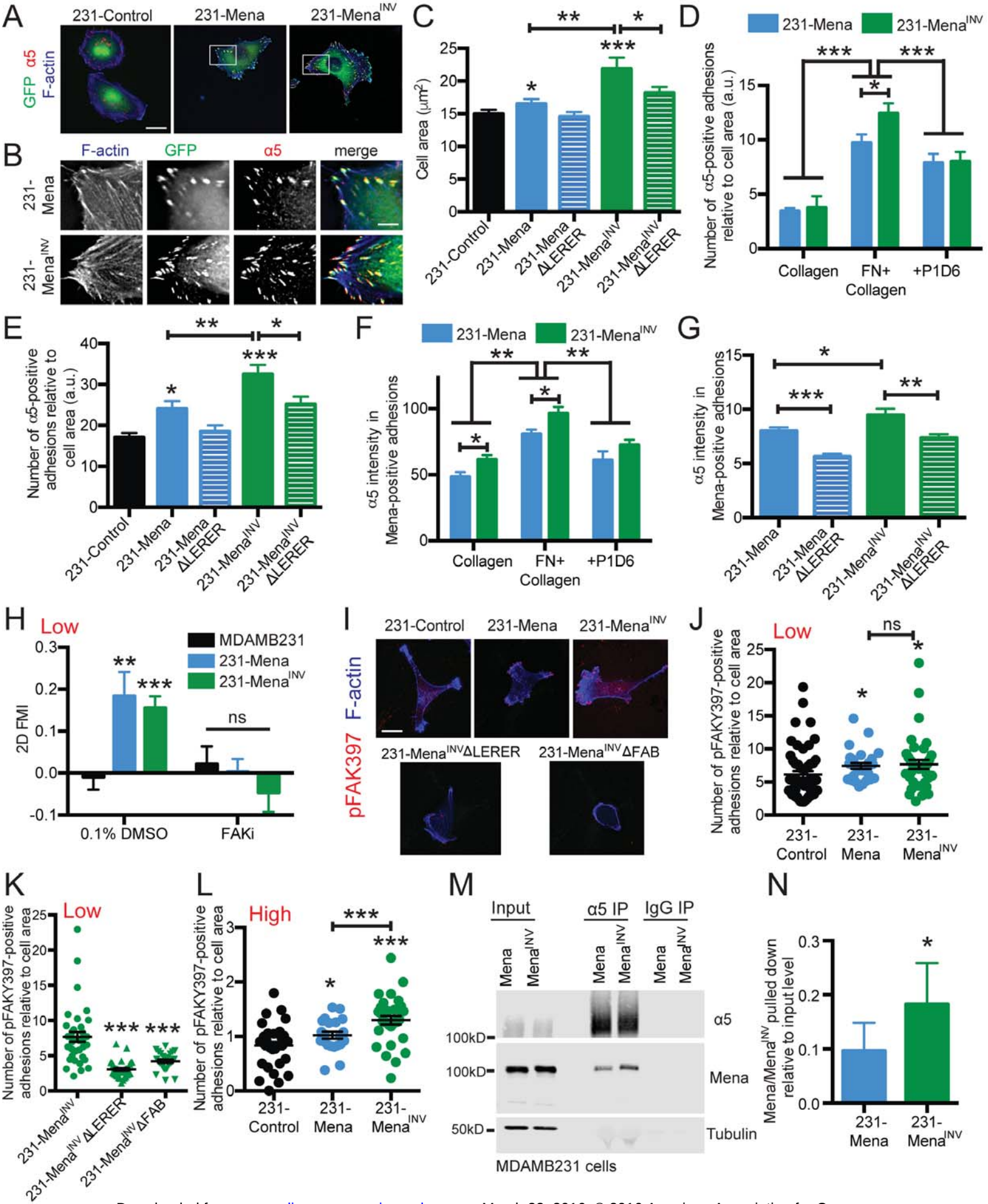

Figure 5

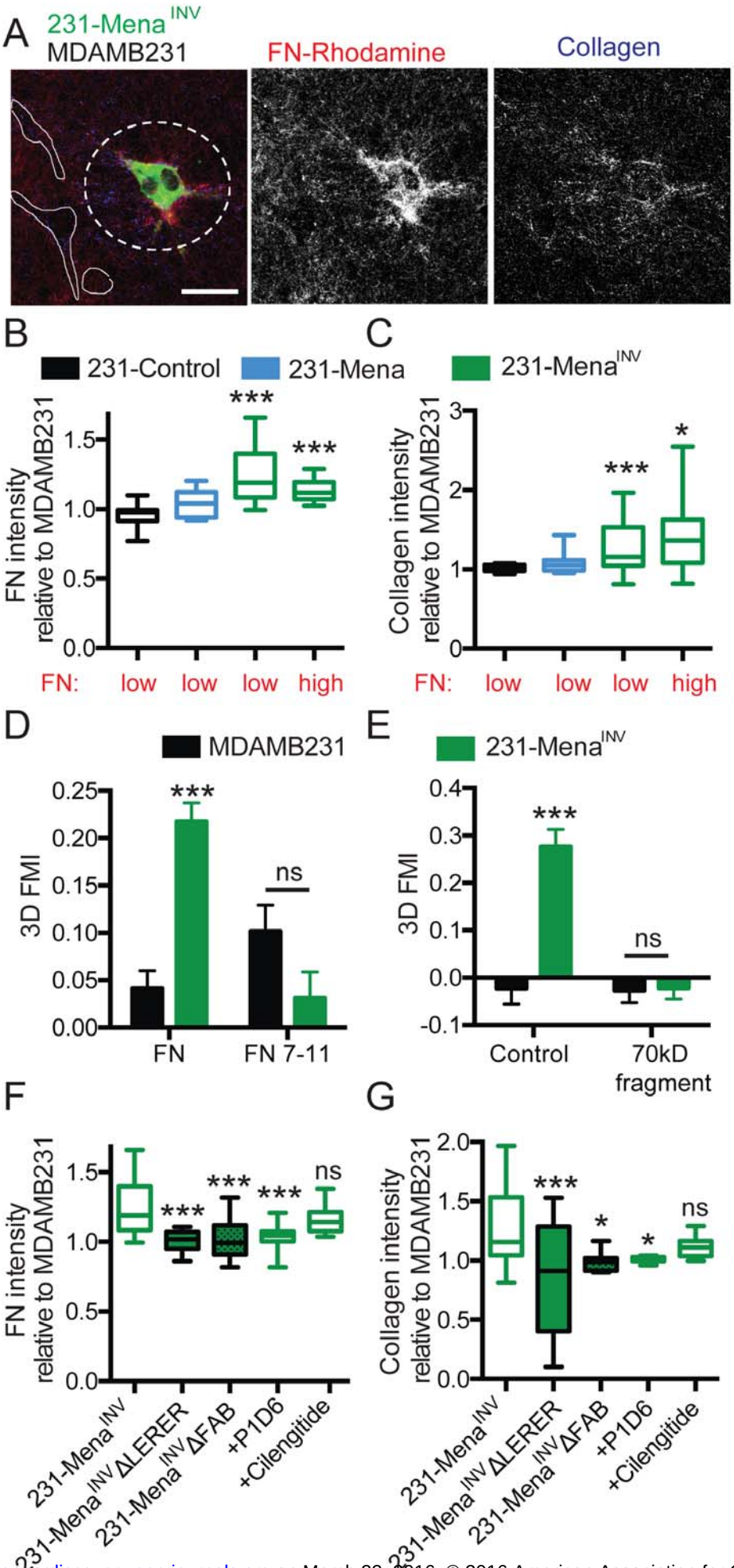

Author Manuscript Published OnlineFirst on January 25, 2016; DOI: 10.1158/2159-8290.CD-15-1183
Author manuscripts have been peer reviewed and accepted for publication but have not yet been edited.

Figure 6

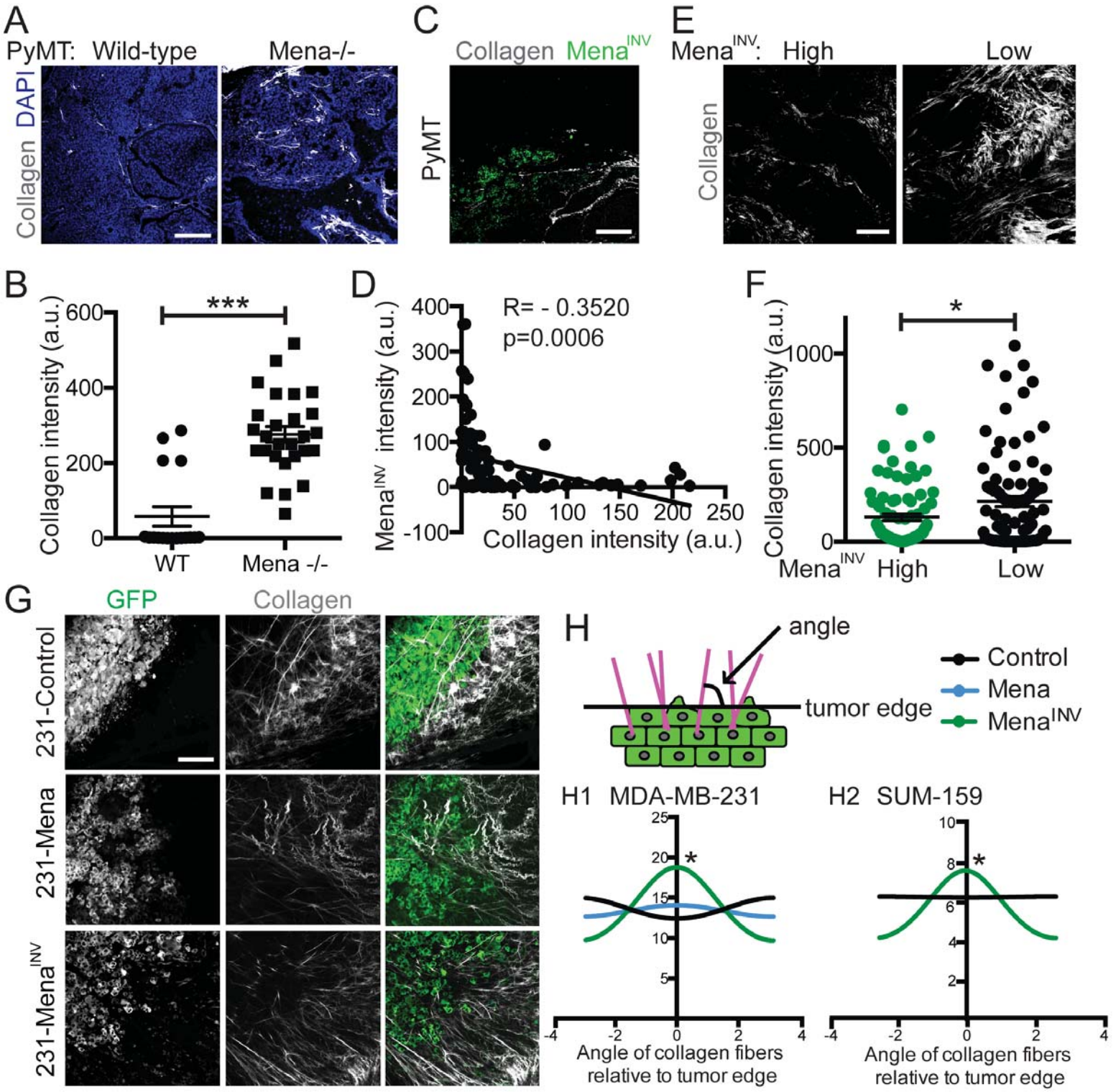

Figure 7

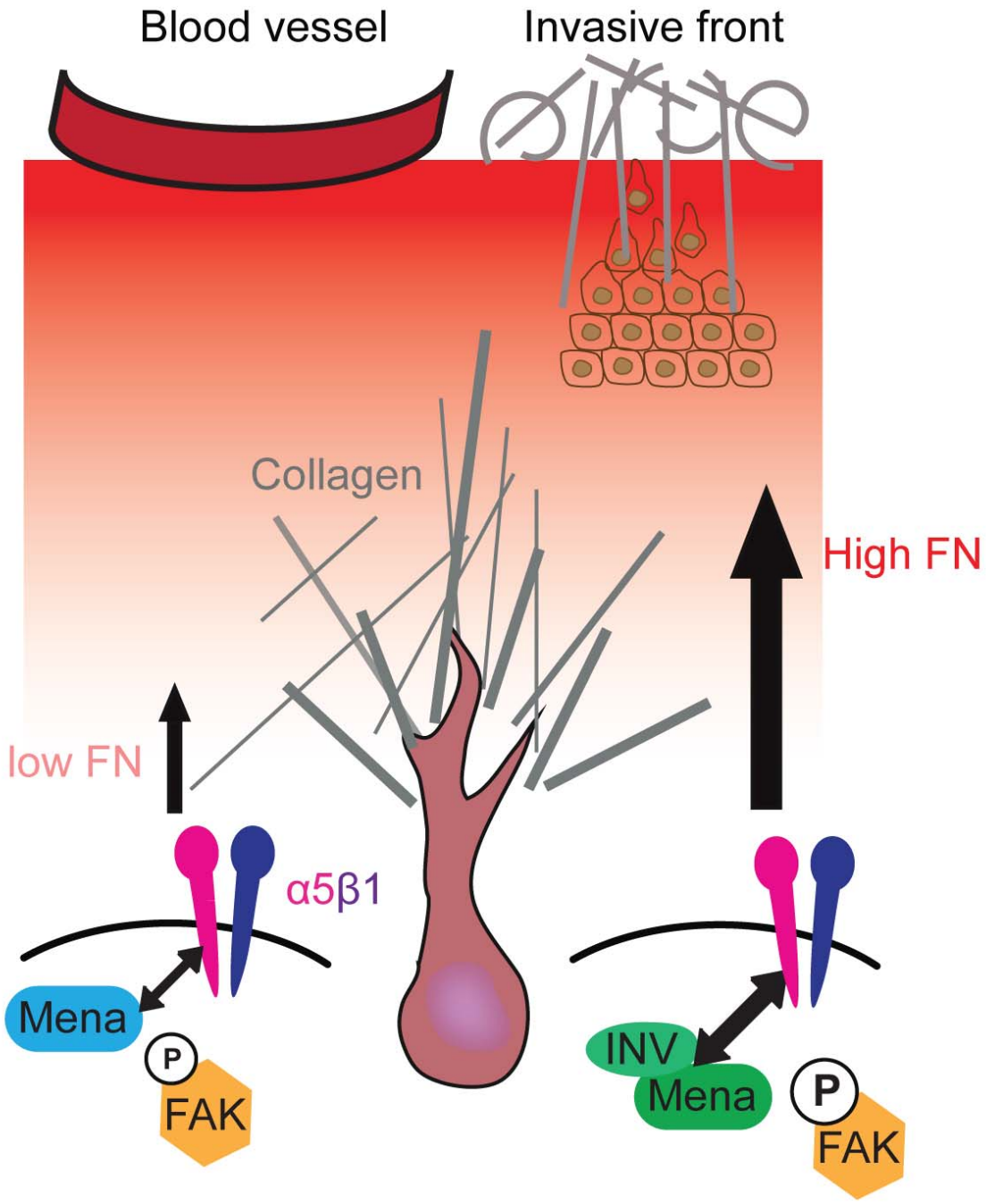

Haptotaxis at ***low*** FN via:
- weak Mena-α5 interaction
- Mena-α5 FX signaling

Haptotaxis at ***high*** FN via:
- stronger Mena-α5 interaction
-increased FX number and signaling
- Collagen + FN reorganization

Low metastatic potential

High metastatic potential

AACR American Association for Cancer Research

CANCER DISCOVERY

Tumor cell-driven extracellular matrix remodeling enables haptotaxis during metastatic progression

Madeleine J. Oudin, Oliver Jonas, Tatsiana Kosciuk, et al.

Cancer Discov Published OnlineFirst January 25, 2016.